small methods

Supporting Information

for *Small Methods,* DOI: 10.1002/smtd.201800539

Lignin-Derived Holey, Layered, and Thermally Conductive 3D Scaffold for Lithium Dendrite Suppression

*Daxian Cao, Qing Zhang, Ahmed M. Hafez, Yucong Jiao, Yi Ma, Hongyan Li, Zheng Cheng, Chunming Niu, and Hongli Zhu**

Supplementary material

Lignin-derived Holey, Layered, and Thermally Conductive 3D Scaffold for Lithium Dendrite Suppression

Daxian Cao[1,2], Qing Zhang[1], Ahmed M. Hafez[1], Yucong Jiao[1], Yi Ma[1], Hongyan Li[1], Zheng Cheng[1], Chunming Niu[2], Hongli Zhu[1,*]

[1]Department of Mechanical and Industrial Engineering, Northeastern University, 360 Huntington Avenue, Boston, Massachusetts 02115, United States

[2]Center of Nanomaterials for Renewable Energy (CNRE), State Key Lab of Electrical Insulation and Power Equipment, School of Electrical Engineering, Xi'an Jiaotong University, Xi'an 710049, China

*: Corresponding author: Hongli Zhu. E-mail: h.zhu@neu.edu

Table of contents:

Part 1. Material synthesis

1.1 The exfoliation process of BN: 0.2 g of Ligninsulfonate (SL) was first dissolved in 20 mL deionized water and then sonicated for 10 min until SL was fully dissolved. 0.2 g BN (Sigma-Aldrich) was then added into the SL solution, and the solution was sonicated for 24 h. The resulted dispersion was centrifuged at 1500 rpm for 15 min to remove the large precipitations of unexfoliated BN. The collected uniform dispersion was transferred to a petri dish, frozen in liquid nitrogen for 5 hours and then froze drying for 3 days. A freestanding aerogel (SL/BN) was formed.

1.2 Electrode preparation process: The carbonization process was performed in the tube furnace under mixed argon/hydrogen (v/v=95/5) flow. Before the carbonization, the obtained aerogel was pressed into a thin and dense film. The aerogel was first heated to 240 ℃ at the heating rate of 5 ℃/min and dwelled at 240 ℃ for 2h. Then it was further heated to 900 ℃ at the heating rate of 10 ℃/min and dwelled for 2 h. A free-standing LHC/BN film was obtained and it was punched into circular disks with a diameter of 6.5 mm to be used as the electrode. The LHC was prepared using the same procedure without the addition of BN and the exfoliation process. Cu foil from MTI was washed in acetone under sonication, and then punched into circular with same diameter to be used as a controlled electrode.

Part 2. Electrochemical Measurements

In the electrochemical measurement, CR2025-type two-electrode coin cells were assembled in an argon-filled glove box. The electrolyte used in the test was 1 M Li bis(trifluoromethanesulphonyl)-imide (LiTFSI) dissolved in DOL/DME (1:1 v/v) with 2 wt.%

lithium nitrate. The separator used in all cells was Celgard 2325 (25 μm thickness). A LANDTH 8-channel tester was used for the galvanostatic test. EIS was conducted using Biologic VMP3 potentiostat.

2.1 Coulombic efficiency: In the Coulombic efficiency measurement, LHC/BN, LHC or Cu were used as the working electrode, respectively and Li foil was used as the counter/reference electrode. Prior to test, batteries were cycled between 0.01 and 1 V for 5 cycles at a very low current of 10 μA, in order to form stable SEI on the electrode and remove the surface contamination. Then in each cycle, Li with an areal charge of 1 or 4 mA h cm^{-2} were plated on the LHC/BN, LHC and Cu respectively first, and then stripped to 1V (vs. Li^+/Li), at the same current density. The Coulombic efficiency was calculated based on the ratio of stripping/plating time in each cycle.

2.2 Cycling stability evaluation: In the long term plating/stripping cycle test, Li with areal charge of 5 and 20 mA h cm^{-2} were pre-deposited onto the LHC/BN, LHC and Cu to form LHC/BN-Li, LHC-Li, and Cu-Li anode, respectively. The cells were tested in repeated stripping/plating processes with an areal charge of 1 mA h cm^{-2} at the current density of 1 mA cm^{-2} and with an areal charge of 4 mA h cm^{-2} at the current density of 4 mA cm^{-2}, respectively.

2.3 Full cell performance: In a full cell battery test, LHC/BN-Li, LHC-Li, and Cu-Li with Li amount of 20 mA h cm^{-2} were used as the anode, and the $LiFePO_4$ was used as cathode. The $LiFePO_4$ electrode was prepared by mixing $LiFePO_4$ powder (MTI), carbon black (Sigma-Aldrich), polyvinylidene difluoride (PVDF, Sigma-Aldrich) in the weight ratio of 80:10:10 with N-methyl-2-pyrrolidone (NMP) as the solvent, and then coated onto Al foil with a mass loading of 3 mg cm^{-2}.

Part 3. Materials and Electrochemical Characterizations

X-ray diffraction (XRD) patterns of the samples were recorded for two θ ranging from 10° to 80° on PANalytical/Philips X'Pert Pro with Cu Kα radiation. Raman spectra was obtained on a LabRam HR800 UV NIR with 532 nm laser excitation. SEM was performed on a Hitachi S4800 SEM. TEM and HRTEM images were performed on the JEOL 2010. DLS was measured on the Brookhaven instruments limited system with a model BI-200SM goniometer, a model BI-900AT digital correlator, and a model EMI-9865 photomultiplier (Lexel Corp.). Thermal diffusivity was measured with the Netzsch LFA 457 MicroFlash.

Part 4. Supplementary Figures

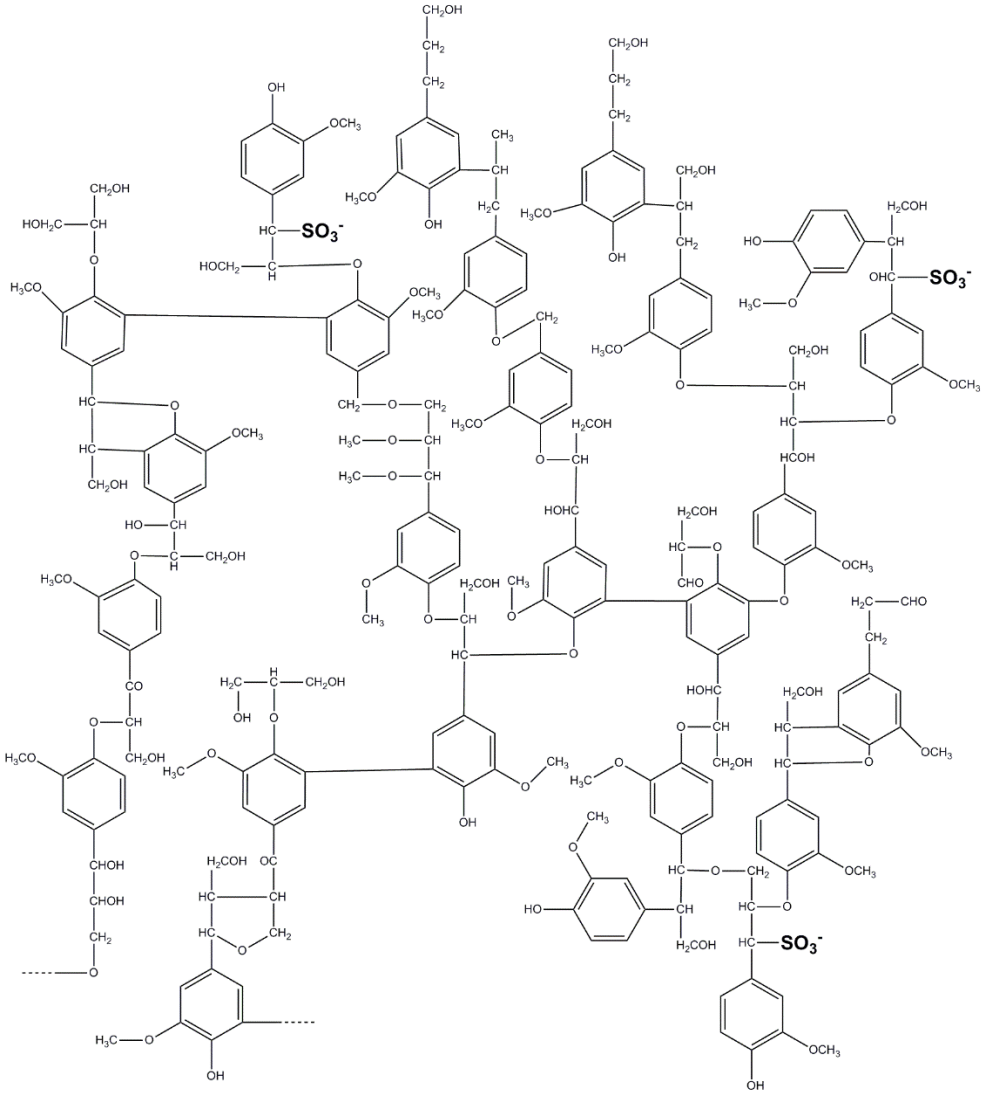

Figure S1. Molecular structure of SL to show the carbon backbone and various function groups, including sulfonic, carboxyl and phenolic hydroxyl groups.

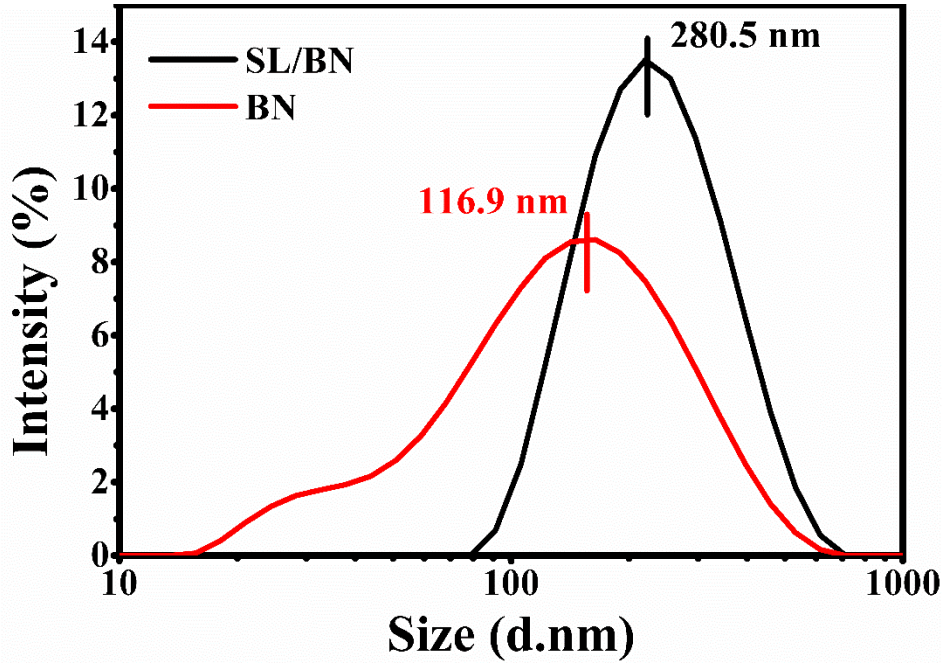

Figure S2. The DLS result shows the size distribution of the BN aqueous dispersion before and after exfoliated by the SL.

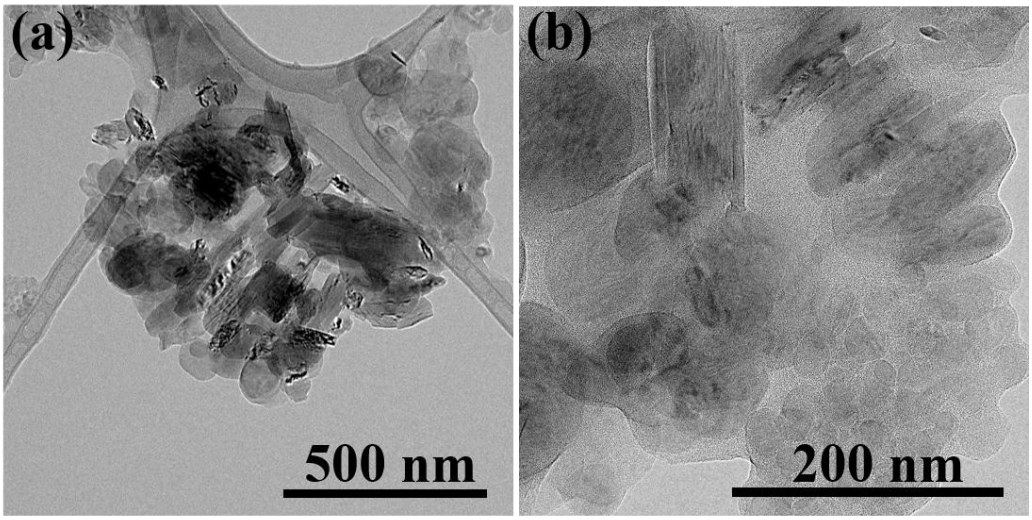

Figure S3. TEM image of bulky BN and exfoliated BN nanosheets with SL;

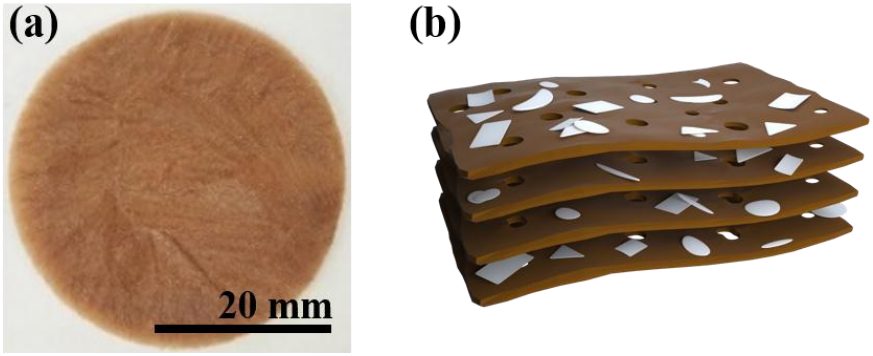

Figure S4. (a) Optical image and (b) schematic of the Lignin/BN aerogel

.

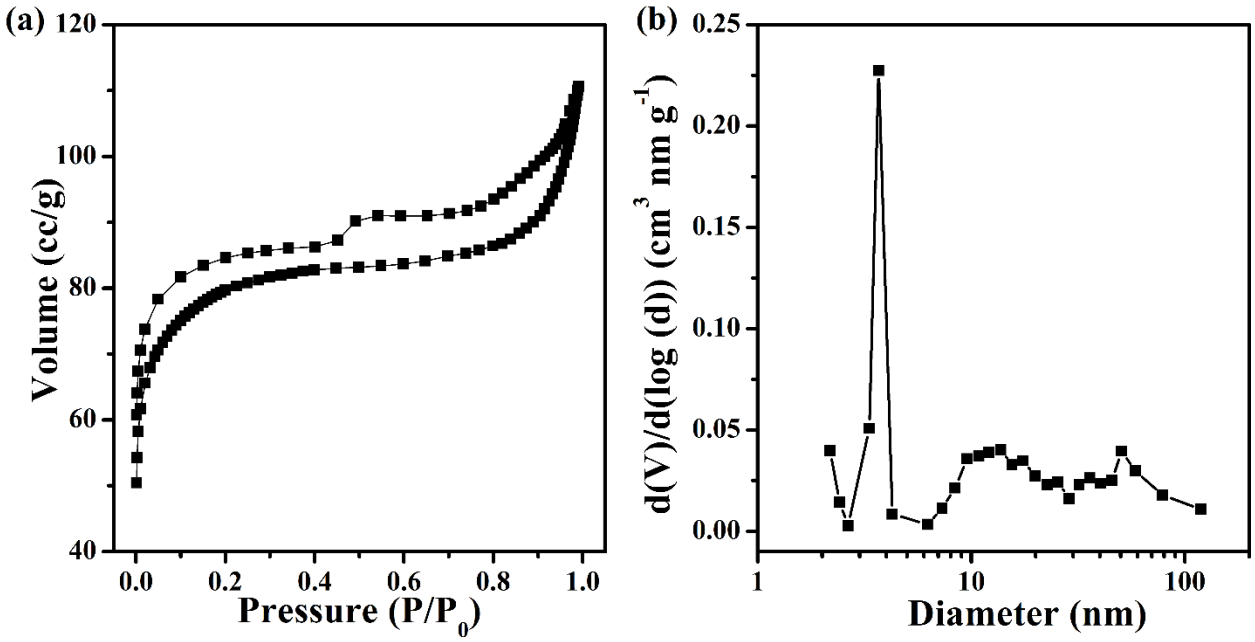

Figure S5. (a) N2 sorption isotherms and (b) the corresponding pore size distribution of the LHC/BN.

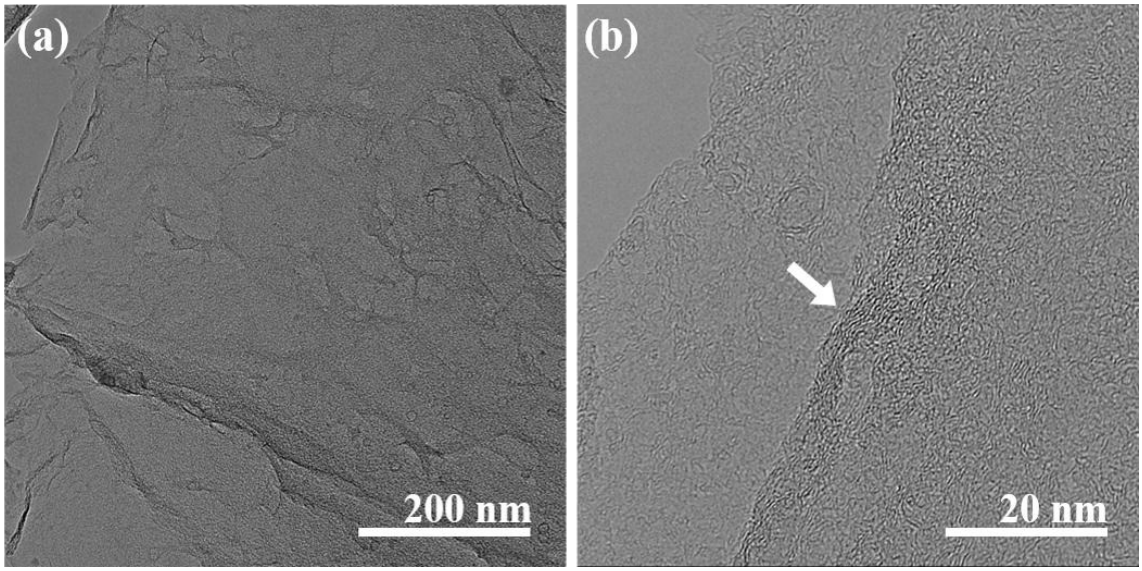

Figure S6. (a) TEM and (b) HRTEM images of LHC.

After the carbonization, SL changed into very thin carbon layers, where most of them are amorphous, and partial crystallized in the edge.

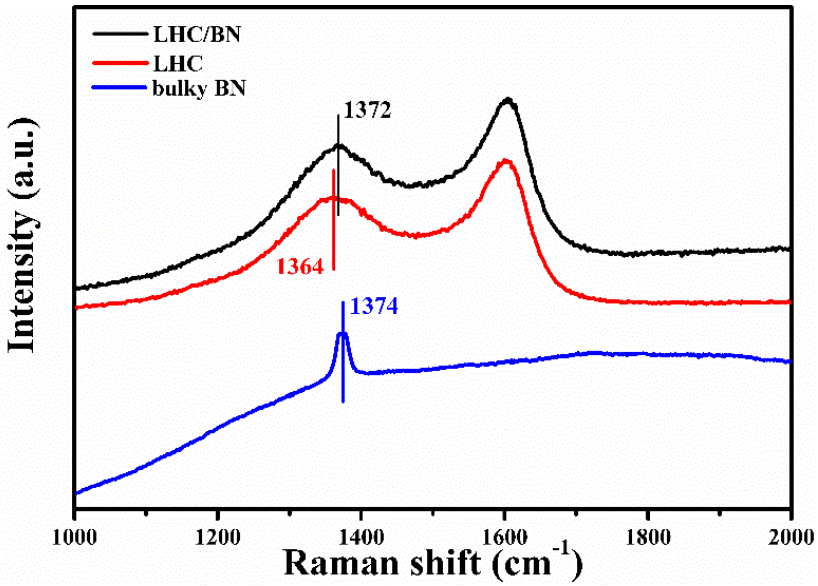

Figure S7. The Raman spectras of the pristine bulky BN (blue line), LHC (red line), and LHC/BN (black line).

There is only one peak appeared at 1374 cm^{-1} belongs to E_{2g} mode peak of h-BN in the pristine bulky BN. In the LHC sample, two prominent peaks at 1364 and 1600 cm^{-1} correspond to D and G bands of carbon derived from SL, respectively. The D band relates to the disordered structure of sp^3 bonded carbon, while G band corresponds to the stretching mode of sp^2 bonded carbon. It shows the amorphous state and partial graphitization of SL after the carbonization. In the LHC/BN sample, the G peak was no change, but D peak shifted a little to 1372 cm^{-1} and become broader, which was owned to the superposition of the D peak of carbon and the peak of BN.

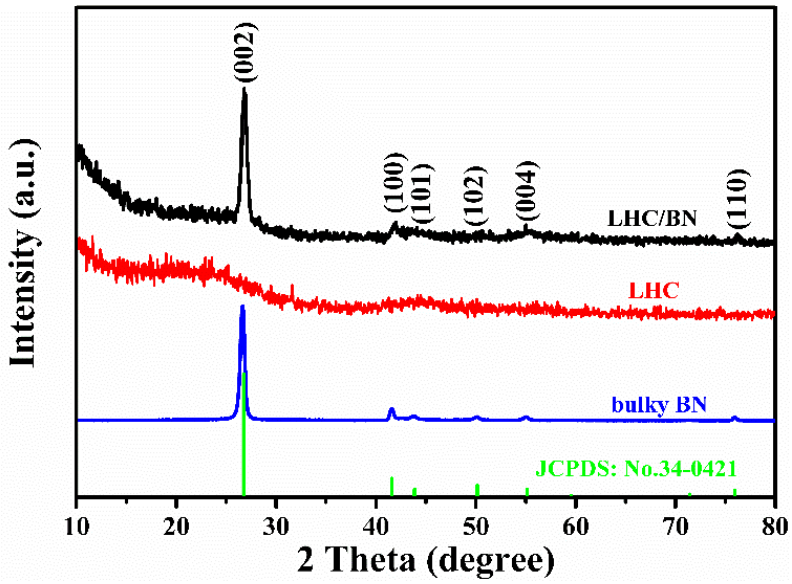

Figure S8. The XRD spectra of the pristine bulky BN (blue line), LHC (red line), and LHC/BN (black line).

The bulky BN has a very good crystalline degree, where the strongest peak located at 27° can be indexed to the (002) plane of h-BN. After exfoliation, the BN nanosheets maintained its good crystallization. The LHC shows a broad peak corresponding to its amorphous state and partial graphitization.

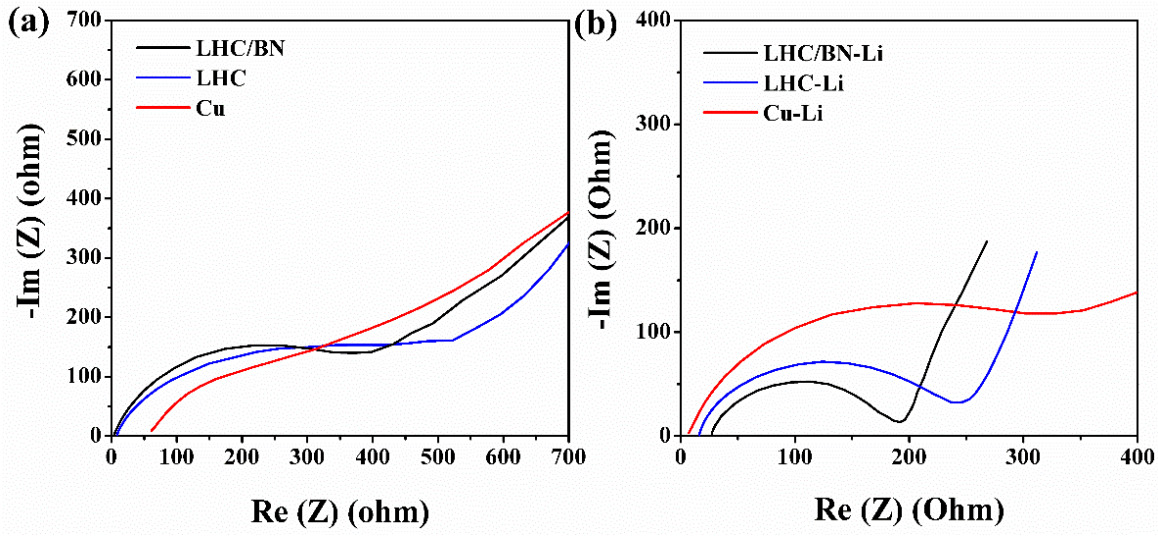

Figure S9. Electrochemical impedance spectroscopy (EIS) for LHC/BN (Black), LHC (Blue) and Cu (Red) (a) Before and (b) after deposition of Li.

It should be mentioned that the diameter of high frequency semicircle represents the charge interfacial resistance at the interface between electrode and electrolyte. It can also evaluate the stability of the SEI layer, the charge transfer speed, and the distribution of electrolyte. Before the Li deposition, LHC/BN, LHC and Cu electrodes own interfacial resistance of 440, 610 and 620 Ω, respectively (Figure S9a). After deposition with Li, the interfacial resistance in LHC/BN-Li, LHC-Li and Cu-Li anodes decrease to 190, 260 and 400 Ω, respectively.

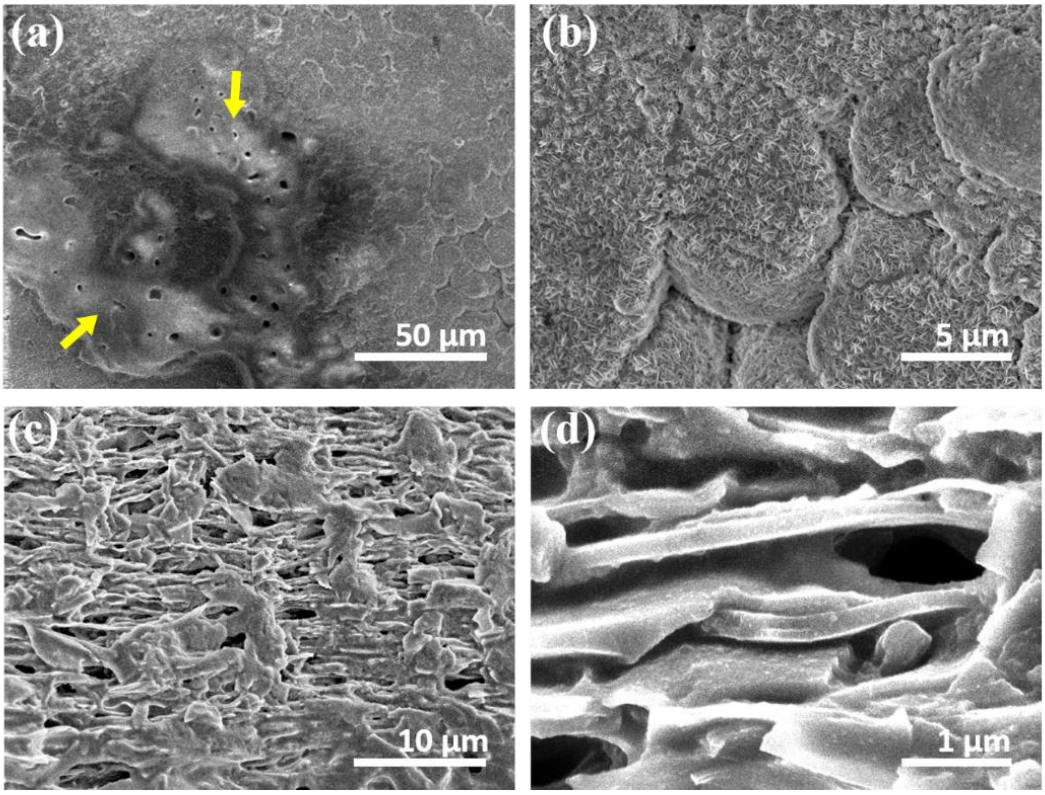

Figure S10. SEM images of LHC-Li before cycling in (a, b) top view and (c, d) side view with different magnification.

After the Li deposition, from the surface image, the district marked with arrows shows the porous structure of LHC, which suggested that the Li have a nonuniform distribution. Zooming in the surface of deposited Li, there are nanosheets existed, and no obvious dendrite can be found. In the side view, the Li were uneven filled in, and some of them grew out from the layers.

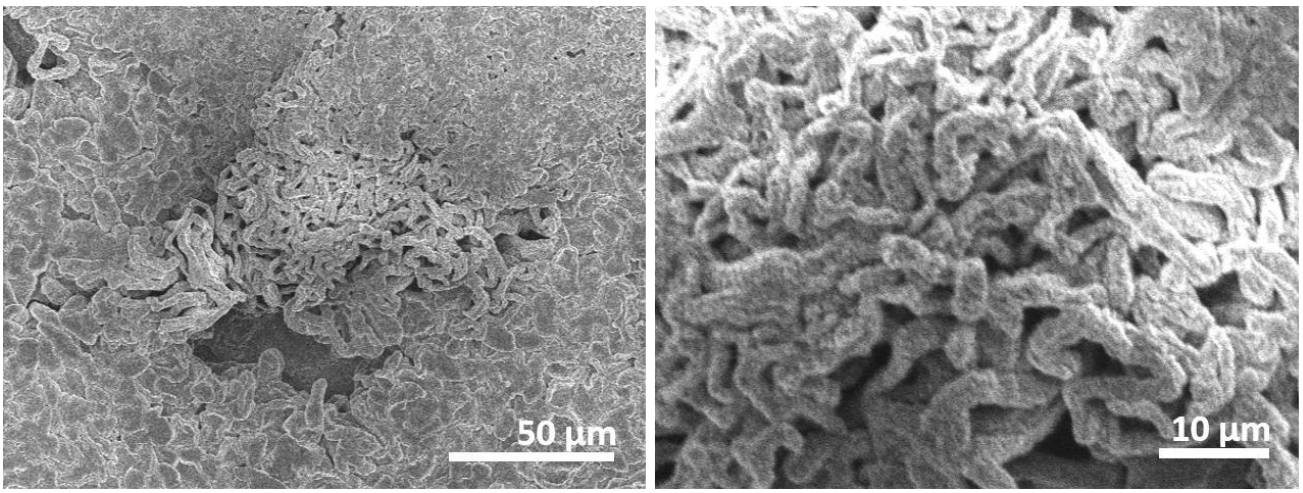

Figure S11. SEM images of Cu-Li in top view with different magnification.

Only deposited Li for 5 hours, there are severe dendrite wires formed on the surface of the Cu-Li.

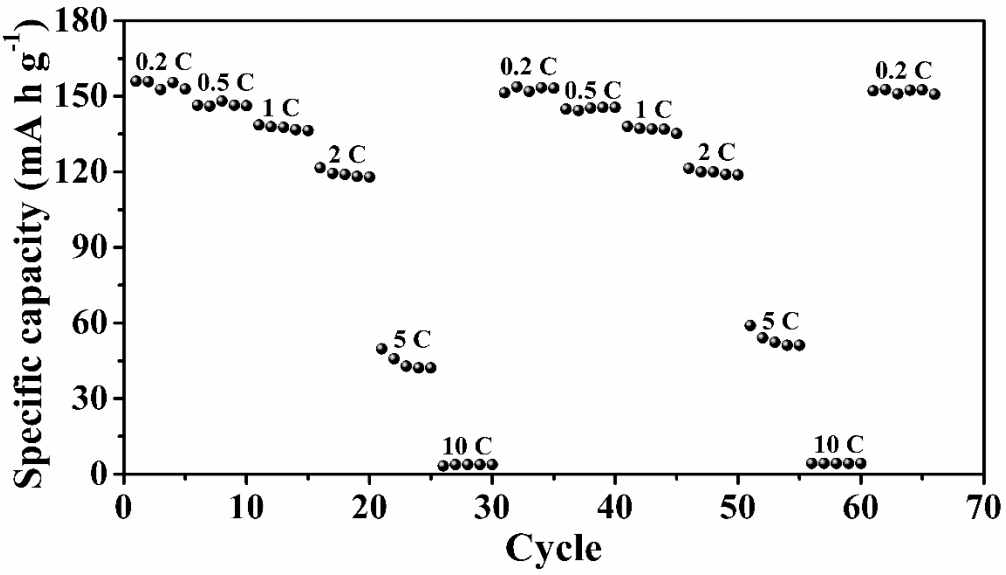

Figure S12. The rate performance of full cell with Li foil as anode.

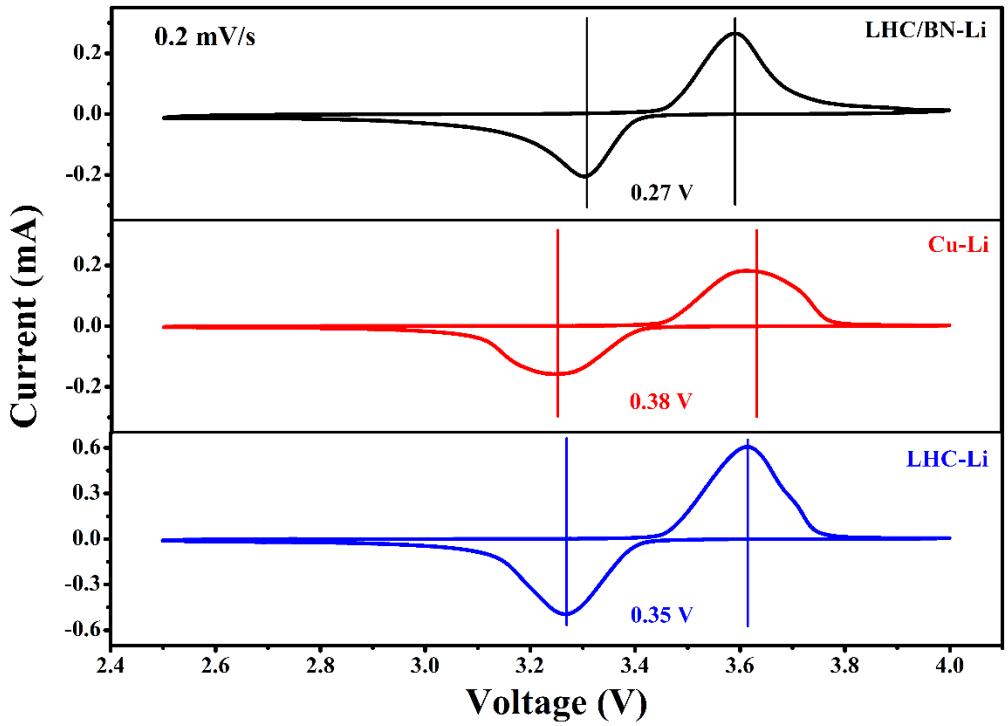

Figure S13. The CV curves of LHC/BN-Li, Cu-Li, and LHC-Li.

It is obvious that the LHC/BN-Li displays the smallest peak separation (the distance of the line), where LHC-Li shows larger, and Cu-Li shows largest. The smaller peak separation indicating smaller polarization in the LHC-BN-Li cell. The CV analysis is consistent with the galvanostatic charge/discharge profiles described in **Figure 6 b-c**. All these data proved that the LHC/BN-Li has excellent charge transfer kinetics.

Part S5. Supplementary Tables.

Table S1. The Coulombic efficiency (CE) of our LHC/BN in comparison with other available lithium host in the literatures.

Host	Current density (mA cm^{-2})	Areal charge (mA h cm^{-2})	CE (%)	cycles	Ref.
LHC/BN	**1**	**1**	**98.5**	**500**	**This work**
	4	**4**	**97.8**	**350**	
Polyacrylonitrile Submicron Fiber	1	1	97.4	250	[1]
CuO on Cu	1	1	94	180	[2]
Poly-melamine-formaldehyde	1	1	89.8	400	[3]
	10	1	94.7	50	
TiC/C	1	1	98.5	100	[4]
Porous Cu	0.5	1	93.8	100	[5]
Porous Cu	1	3	98.5	200	[6]
vapor grown carbon fiber	0.5	2.5	91.1	100	[7]
Porous Ni	2	1	97.5	30	[8]
3D Ni	1	1	99.5	200	[9]
Graphene balls	0.5	0.5	97.49	700	[10]
	1	1	94	50	
Carbon fiber	0.5	2	99.5	350	[11]
	2	4	99	90	
SiO2/CNT	0.5	2	99	200	[12]
3D Cu	0.5	2	90	130	[13]

Table S2. The cycling performance of LHC/BN-Li in comparison with other available lithium host in the literatures.

Host	Current density (mA cm^{-2})	Areal charge (mA h cm^{-2})	Life span (h)	Ref.
LHC/BN	**1**	**1**	**700**	**This work**
	4	**4**	**500**	
Polyacrylonitrile Submicron Fiber	3	3	300	[1]
CuO on Cu	0.5	0.5	700	[2]
Poly-melamine-formaldehyde	2	1	350	[3]
	5	1	80	
	10	1	50	
TiC/C	1	1	200	[4]
	3	1	200	
Porous Cu	1	1	200	[6]
Graphene balls	0.5	1	750	[10]
Carbon fiber	2	1	600	[11]
3D Cu	0.2	0.5	500	[13]
3D Ni foam	1	1	200	[14]
	5	0.2	40	
Carbon cloth	1	1	400	[15]
	5	1	80	
Cu-Ni core-shell wire	3	1	250	[16]
Graphite	1	1.5	600	[17]
	5	1.5	60	
ZnO/Carbon	1	1	400	[18]
	10	1	40	
Graphite carbon	1	1	200	[19]
	3	1	66	
Coralloid Carbon Fiber	1	1	400	[20]
Wood	1	1	330	[21]
	3	1	450	

Table S3. Full cell performance of LHC/BN-Li in comparison with other available Li anode with host in the literatures, with $LiFePO_4$ as cathode. Here 1C means 170 mA h g^{-1}.

Anode	Current density (mA g^{-1})	Specific capacity (mA h g^{-1})	Cycle number	Capacity retention (%)	Ref.
LHC/BN-Li	**1700**	**90**	**1800**	**92**	**This work**
Polyacrylonitrile Submicron Fiber with Li	85	120	300	82	[2]
Poly-melamine-formaldehyde with Li	850	126	200	91	[4]
Porous Cu with Li	85	134	100	90	[6]
Graphene balls with Li	85	~130	200	91	[11]
3D Cu with Li	170	131	250	99	[13]

Reference

[1] J. Lang, J. Song, L. Qi, Y. Luo, X. Luo, H. Wu, *ACS Appl Mater Interfaces* **2017**, 9, 10360.

[2] Z. Chen, L. Wei, Z. Guangmin, H. Zhijia, Z. Yunbo, L. Ruiyang, W. Haoliang, Y. Qinbai, K. Feiyu, Y. Quan‐Hong, *Advanced Energy Materials* 0, 1703404.

[3] F. Lei, Z. H. L., Z. Weidong, F. Yao, L. Zhihao, L. Yingying, *Advanced Energy Materials* **2018**, 8, 1703360.

[4] L. Sufu, X. Xinhui, Z. Yu, D. Shengjue, Y. Zhujun, Z. Liyuan, C. Xin‐Bing, W. Xiuli, Z. Qiang, T. Jiangping, *Advanced Energy Materials* **2018**, 8, 1702322.

[5] L. Qi, Z. Shoupu, L. Yingying, *Adv Funct Mater* **2017**, 27, 1606422.

[6] W. Shu‐Hua, Y. Ya‐Xia, Z. Tong‐Tong, D. Wei, L. Jin‐Yi, S. Ji‐Lei, Z. Chang‐Huan, L. Nian‐Wu, L. Cong‐Ju, G. Yu‐Guo, *Advanced Materials* **2017**, 29, 1703729.

[7] Y. Yang, J. Xiong, J. Zeng, J. Huang, J. Zhao, *Chemical Communications* **2018**, 54, 1178.

[8] Y. Lu, C. N. L., C. Shuru, L. Hongkyung, R. Xiaodi, E. M. H., L. Qiuyan, L. Jun, X. Wu, Z. Ji‐Guang, *ChemElectroChem* **2018**, 5, 761.

[9] Y. Xu, A. S. Menon, P. P. R. M. L. Harks, D. C. Hermes, L. A. Haverkate, S. Unnikrishnan, F. M. Mulder, *Energy Storage Materials* **2018**, 12, 69.

[10] S. Liu, A. Wang, Q. Li, J. Wu, K. Chiou, J. Huang, J. Luo, *Joule* **2018**, 2, 184.

[11] L. Liu, Y.-X. Yin, J.-Y. Li, N.-W. Li, X.-X. Zeng, H. Ye, Y.-G. Guo, L.-J. Wan, *Joule* **2017**, 1, 563.

[12] T.-T. Zuo, Y.-X. Yin, S.-H. Wang, P.-F. Wang, X. Yang, J. Liu, C.-P. Yang, Y.-G. Guo, *Nano Lett* **2018**, 18, 297.

[13] P. Zou, Y. Wang, S.-W. Chiang, X. Wang, F. Kang, C. Yang, *Nat Commun* **2018**, 9, 464.

[14] C. Shang‐Sen, L. Yongchang, S. Wei‐Li, F. Li‐Zhen, Z. Qiang, *Adv Funct Mater* **2017**, 27, 1700348.

[15] Y. Zhou, Y. Han, H. Zhang, D. Sui, Z. Sun, P. Xiao, X. Wang, Y. Ma, Y. Chen, *Energy Storage Materials* **2018**, 14, 222.

[16] L.-L. Lu, Y. Zhang, Z. Pan, H.-B. Yao, F. Zhou, S.-H. Yu, *Energy Storage Materials* **2017**, 9, 31.

[17] S. Liu, X. Xia, S. Deng, L. Zhang, Y. Li, J. Wu, X. Wang, J. Tu, *Energy Storage Materials* **2018**, 15, 31.

[18] L. Wang, X. Zhu, Y. Guan, J. Zhang, F. Ai, W. Zhang, Y. Xiang, S. Vijayan, G. Li, Y. Huang, G. Cao, Y. Yang, H. Zhang, *Energy Storage Materials* **2018**, 11, 191.

[19] J. Lang, Y. Jin, X. Luo, Z. Liu, J. Song, Y. Long, L. Qi, M. Fang, Z. Li, H. Wu, *Journal of Materials Chemistry A* **2017**, 5, 19168.

[20] R. Zhang, X. Chen, X. Shen, X.-Q. Zhang, X.-R. Chen, X.-B. Cheng, C. Yan, C.-Z. Zhao, Q. Zhang, *Joule* **2018**, 2, 764.

[21] Y. Zhang, W. Luo, C. Wang, Y. Li, C. Chen, J. Song, J. Dai, E. M. Hitz, S. Xu, C. Yang, Y. Wang, L. Hu, *Proceedings of the National Academy of Sciences* **2017**, 114, 3584.